Journal of Advanced Joining Processes 8 (2023) 100156

Contents lists available at ScienceDirect

Journal of Advanced Joining Processes

journal homepage: www.sciencedirect.com/journal/journal-of-advanced-joining-processes

Robotic friction stir welding in lightweight battery assembly of extrusion-cast aluminium alloys

Vivek Patel [a,*], Hendrik Wouters [a], Amir Baghdadchi [a,*], Jeroen De Backer [a,b], Mattias Igestrand [a], Saeed Azimi [c], Joel Andersson [a]

[a] Department of Engineering Science, University West, Trollhättan 46186, Sweden
[b] Friction & Forge Processes, TWI, Cambridge CB21 6AL, UK
[c] Volvo Car Corporation, Gothenburg 41878, Sweden

ARTICLE INFO

Keywords:
Stationary shoulder friction stir welding
Aluminium alloys
HPDC
Extrusion
Lightweight
BEV

ABSTRACT

The present study focuses on developing lightweight assembly of two different aluminium alloys extruded and high pressure die cast (HPDC) for battery frame assembly in BEV. The goal is to produce defect-free welds in lap configuration with smooth surface finish. Stationary shoulder friction stir welding (SSFSW) was employed with welding speeds of 3–15 mm/s. EBSD analysis revealed two groups of grains in the stir zone (SZ) due to dynamic recrystallization. Moreover, the grain size of the SZ significantly decreased compared to both alloys. The cast alloy contains large iron particles, and that were broken by the rotating probe, and the stirred material consisted of fine dispersed precipitates. Tensile-shear test found the fracture location at the hook area near to cast, and a model representing fracture behavior is also discussed. With increasing welding speed from 3 to 5 mm/s, the tensile strength found ~95 and ~100 MPa, respectively without any significance difference in the fracture behavior and location. Overall, this study provides valuable insights such as materials mixing, grain refinement, and joint strength in dissimilar joining using SSFSW. The findings could be useful in developing optimized welding parameters and improving the overall quality and productivity of the SSFSW process for battery pack assembly in BEV.

Introduction

The shift towards sustainable development and green transition is affecting the automotive industry in significant ways, with a particular emphasis on the transition to battery electric vehicles (BEV). One important aspect of this shift is the need to reduce the weight of vehicles to improve energy efficiency and reduce emissions. Aluminium alloys, with their high strength-to-weight ratio, excellent corrosion resistance, and recyclability, are a promising material for achieving this goal. The use of aluminium alloys in the automotive industry is not new, but ongoing research is exploring new alloys and fabrication processes that can improve their properties and reduce their environmental impact. Aluminium 6xxx series, for example, is a popular choice due to its high strength, excellent corrosion resistance, and extrudability. High pressure die cast (HPDC) aluminium alloys, on the other hand, offer a unique combination of properties that make them particularly suitable for certain applications, such as battery box assembly in BEVs. HPDC aluminium alloys can help to reduce the weight of parts, lower manufacturing costs, and achieve fine surface finishes. Additionally, they offer excellent dimensional stability, even at high temperatures, which is critical for certain applications in the automotive industry. By leveraging the unique properties of different aluminium alloys, researchers and manufacturers can develop innovative solutions that meet the needs of the industry while advancing sustainable development goals.

Indeed, welding is a primary method of joining different materials, including aluminium alloys (Xu et al., 2018). It has been reported about recent developments in friction stir welding (FSW), explanining several drawbacks of traditional fusion welding techniques for aluminium alloys (Çam and Mistikoglu, 2014). It is also discussed fusion welding challenges such as solidification cracking, formation of porosities, and distortions in aluminium alloys. Recently, Sejani et al. (2021) published comprehensive review article on friction stir welding tooling system, where they mentioned issues and challenged related to dissimilar materials welding. One of the common issues they pointed out is a risk of the formation of brittle intermetallic compounds, which can

* Corresponding authors.
E-mail addresses: vivek.patel@hv.se (V. Patel), amir.baghdadchi@hv.se (A. Baghdadchi).

https://doi.org/10.1016/j.jajp.2023.100156

Available online 22 September 2023

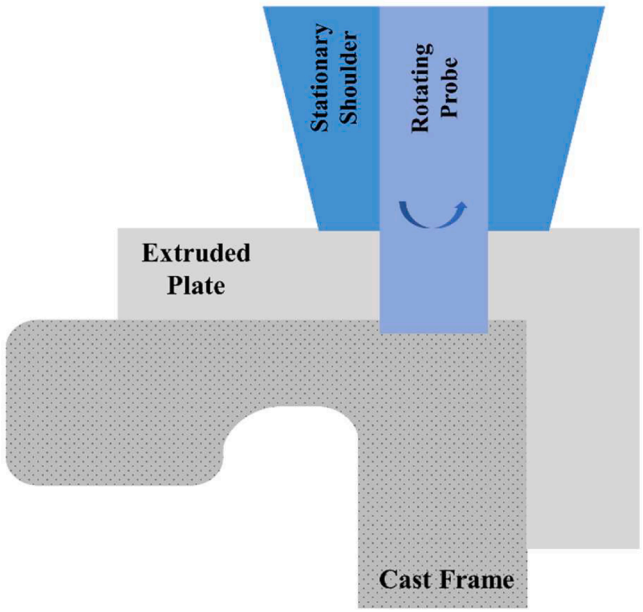

Fig. 1. Schematic illustration of battery frame assembly consisting of cast structure and extrusion plate.

compromise the mechanical properties of the joint. Thomas et al. (1991) invented FSW as a solid-state welding technique that joins materials together by applying frictional heat using a non-consumable rotating tool. Mishra and Ma (2005) demonstrated about heat generation during the FSW. They stated that heat is generated by the frictional force that softens the material, which allows the tool to stir the softened material for producing a sound joint. Since FSW is a solid-state process, which does not allow melting or solidification of the material, thereby eliminating the risk of solidification cracking and porosity formation, as reported by Besharati-Givi and Asadi (2014). Additionally, FSW is considered a more sustainable and environmentally friendly process compared to conventional fusion welding, as there are no toxic gases or fumes generated during the process. Therefore, FSW is a promising technique for joining dissimilar alloys, such as aluminium 6063-T6 and HPDC Al-4Mg-2Fe, for battery box assembly in BEVs. The technique can provide a leakproof and sound joint with excellent mechanical properties, while also being more environmentally friendly compared to traditional welding techniques.

The literature for FSWed lap joints of aluminium alloys reported effect of process parameters on the weld defects. Aldanondo et al. (2017) compared two different thread probes at different welding parameters for AA-7075-T6 alloys and concluded that the three-flats pin improves the stirring and material flow resulting in the smaller hook defects. Song et al. (2014) studied the dissimilar welding of AA2024-T3 and AA7075-T6 alloy sheets in lap configuration by FSW to investigate the effects of lapping sequence and welding speed on the defects and mechanical properties of the welds. They found that the hook feature varies with both the welding speed and the lapping sequence, which governs the joint strength. In another study, Dinaharan et al. (2012) investigated effect of joint configuration and tool rotational speed in the butt FSW of 6-mm cast to wrought AA6061 plates, and argued that the SZ mostly contains the material was placed in advancing side and same can be enhanced by increasing the tool rotational speed. The best tensile strength was also achieved when the cast aluminium alloy was on the advancing side.

Stationary shoulder friction stir welding (SSFSW) is a variant of FSW where the shoulder remains stationary while the rotating pin generates frictional heat that softens the material and allows it to be stirred together to form a bond. Barbini et al. (2018) exhibited SSFSW of dissimilar high strength aluminium alloys AA2024/AA7075 and concluded that stationary shoulder results in a more symmetrical joint with a narrow heat affected zone (HAZ) and thermomechanical affected zone (TMAZ). Which helps in producing a more homogeneous microstructure with less softening effect. Additionally, because the shoulder does not rotate, the forging force is reduced, preventing weld thinning and resulting in a finer weld surface as reported by Ahmed et al. (2011).

Welding of wrought aluminium alloy to cast aluminium alloy is indeed challenging due to the differences in their material properties, especially when defects such as entrapped air and shrinkage porosities are present in the cast aluminium. FSW is a promising method for joining these two alloys, and SSFSW in lap configuration is expected to be a suitable approach for the battery frame assembly. The use of HPDC aluminium alloy for the battery frame assembly is also interesting, as it allows for the development of large and complicated design structures as a single component. The battery frame assembly consists of casting frame and extruded plates, and the cast frame is sealed by placing extrusion plates on the top using FSW, as schematically represented in Fig. 1. The lap joint configuration of extruded aluminium 6063-T6 and HPDC Al-4Mg-2Fe for the battery frame structure in BEV can provide a cost-effective solution while maintaining strength and corrosion resistance.

Therefore, the key objective of the present study is to explore SSFSW of extruded aluminium 6063-T6 to HPDC Al-4Mg-2Fe in lap configuration, as there is limited literature available on this specific combination of alloys. Moreover, the present study can provide valuable insights into the feasibility and effectiveness of using SSFSW for joining these two alloys and can potentially lead to the development of cost-effective and high-quality battery box assemblies for BEVs.

Materials and methods

In this study, two 3-mm aluminium sheets, the wrought Al 6063-T6 and a new HPDC Al-4Mg-2Fe, were welded in the lap configuration by SSFSW. The Al 6063-T6 sheet was on the retreating side and the HPDC

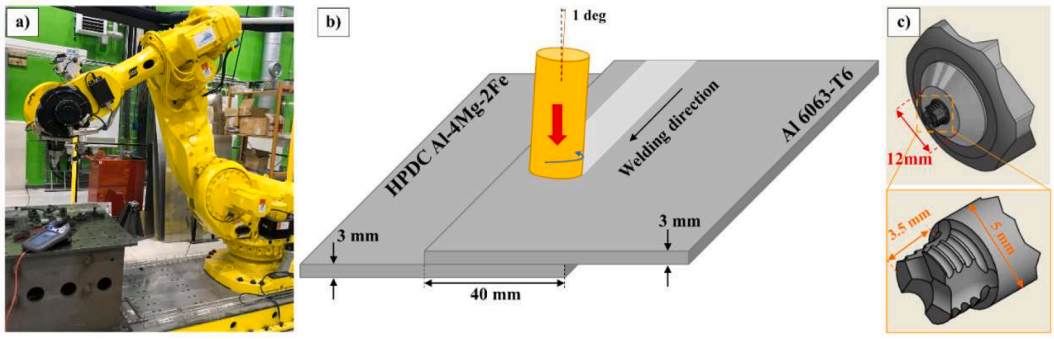

Fig. 2. (a) FSW setup, (b) dimensions of the aluminium plates for SSFSW and (c) the schematic illustration of the stationary shoulder and three-flute crown pin.

Table 1
The welding parameter of SSFSW of aluminium alloys.

Weld #	Rotational speed (rpm)	Force (N)	Welding speed (mm/s)
S1	2000	5000	15
S2	2000	4000	10
S3	2000	4500	10
S4	2000	4000	5
S5	1500	4000	3
S6	2000	4000	3

was on the advancing side. All welds are made using a robotic FSW system at the Production Technology Center (PTC) in Trollhättan, Sweden. The robotic system consists of an ESAB Rosio serial kinematics robot 5-axis robot equipped with a spindle motor, force sensor, temperature measurement and a control system as presented in Fig. 2. The SSFSW tool was composed of two main parts: (i) rotating probe or pin and (ii) non-rotating shoulder. The schematic illustrations of both probe and shoulder made from H13 tool steel are shown in Fig. 2. The threaded probe with three-flute crown was used for better mixing and breaking the aluminium oxides on the cast plate surfaces to eliminate pre-brushing. The height and diameter of the probe and the diameter of the stationary shoulder were 3.5 mm, 5 mm and 12 mm, respectively.

A total of six welds were produced in lap configuration and the SSFSW parameters are presented in Table 1. The SSFSW was performed with various forces, tool rotational speeds and welding speeds. The combination of these parameters is selected in such a way to prevent the probe failure in stationary shoulder tooling system. The tilt angle of the axis was 1° for all SSFSW lap joints.

After welding, the cross-sections of all welds were mounted, ground, and polished down to 0.05 μm using alumina suspension in the last step. To reveal different zones in the weld and to study the macrostructure, the samples were etched using Kellar's reagent. After etching samples were investigated under a light optical microscope using Zeiss Axio Imager 2 for any kind of defects formed during welding. A ZEISS Gemini Scanning Electron Microscopy (SEM) 450 was used for studying the microstructures of the base materials, stir zone and fracture surfaces. The SEM was equipped with an Energy Dispersive Spectroscopy (EDS) for chemical analysis and with a Symmetry S2 EBSD detector from Oxford Instruments for phase and crystal orientation analysis. For EBSD analysis, the acceleration voltage, sample tilt angle, and working distance were 15 kV, 70̊, and 8.5 mm, respectively. Step sizes were 0.06 μm and 1.5 μm for weld (stir zone) and BMs, respectively. The AZtecCrystal 1.1 software from Oxford Instruments was used to analyze the EBSD results.

Once after completing the microscopic study on the samples, the samples were ground and polished thoroughly to perform the Vickers hardness test. The Vickers hardness measurement was performed with a Struers Duramin-40 with a load of 200 gf, a dwell time of 10 s and a minimum distance of 0.5 mm between two test points. Hardness mapping was produced by taking 400–500 indentations covering the stir zone (SZ), thermomechanical affected zone (TMAZ), heat affected zone (HAZ), and base material (BM). The static mechanical strength of the SSFSW lap joints was investigated by the lap shear tensile test on the selected specimens. To evaluate the homogeneity of tensile properties in

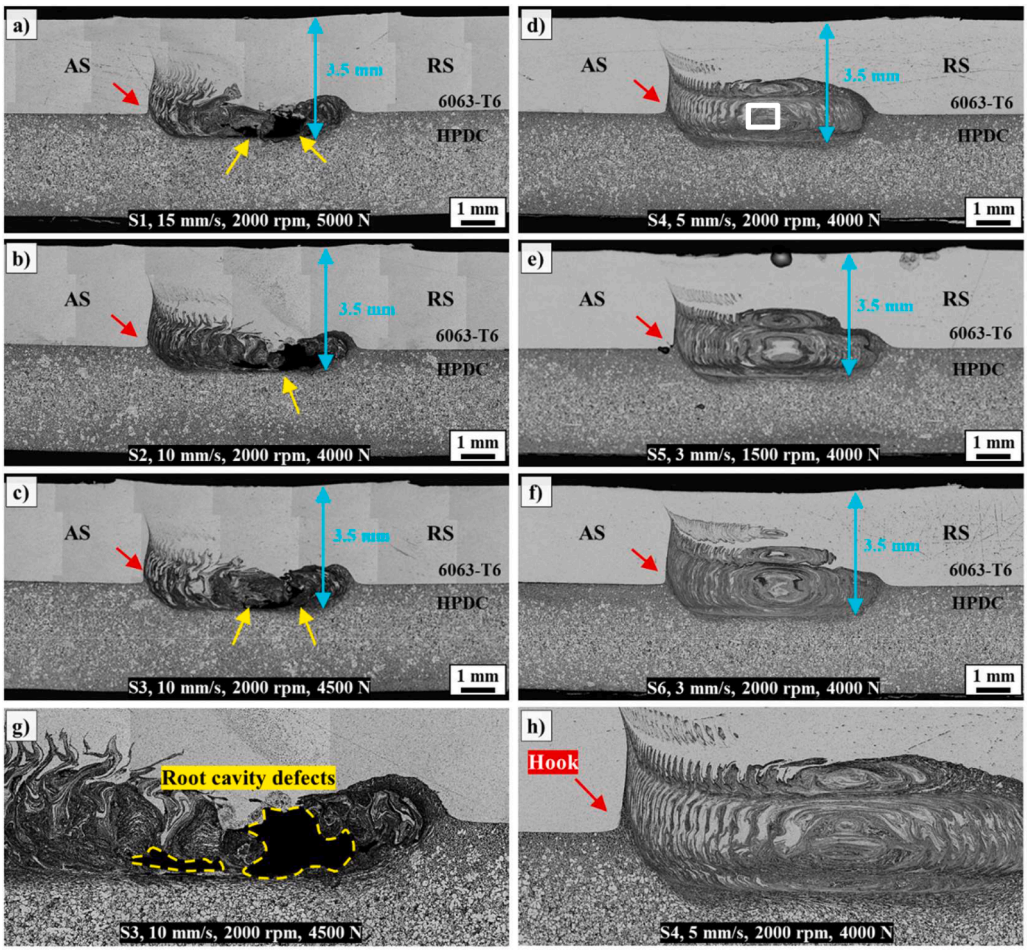

Fig. 3. Weld Cross-sections of the all samples representing material mixing with same depth of penetration: (a) S1, (b) S2, (c) S3, (d) S4, (e) S5, and (f) S6; (g) closer look of root cavity of S3 and (h) closer look of hook of S4.
Note: arrow with red color showing hook on AS and arrow with yellow color revealing voids at the root.

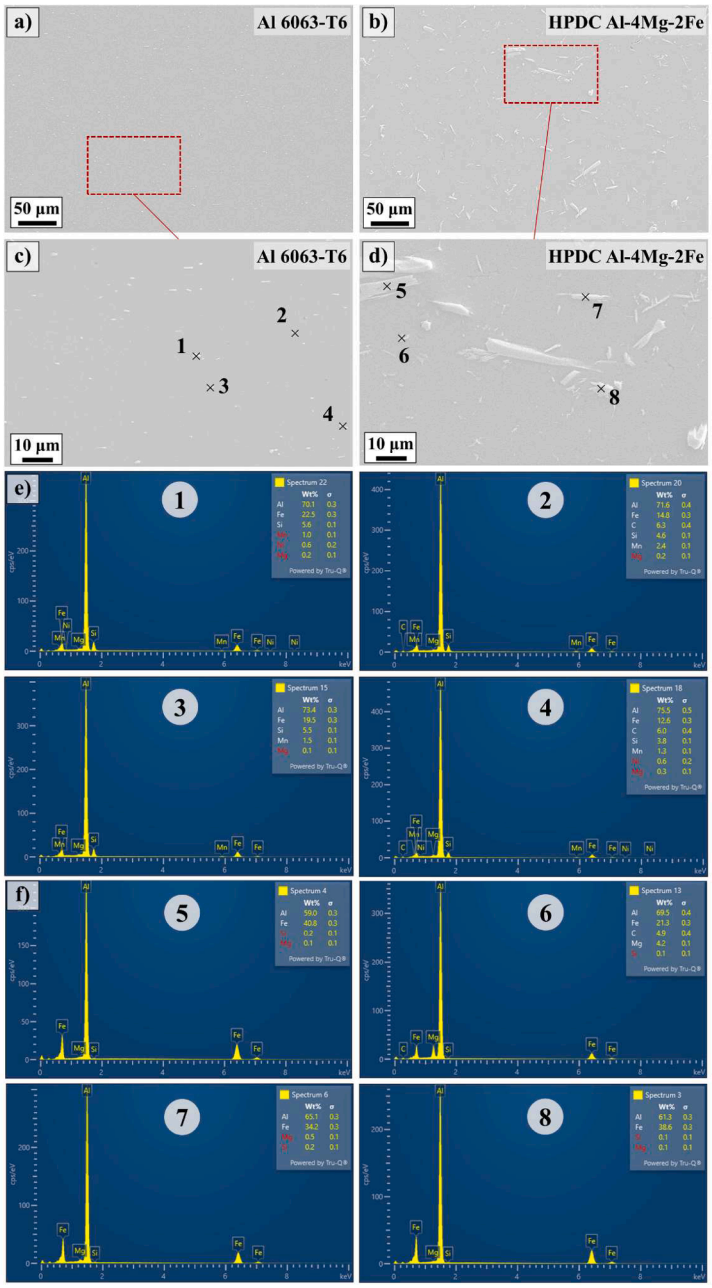

Fig. 4. The SEM micrographs of (a and c) extruded aluminium 6063-T6, and (b and d) HPDC Al-4Mg-2Fe. (e and f) SEM-EDS analysis of the points in c and d.

both directions and check the fracture location, the samples were pulled from both AS and RS sides. All tests were performed by Zwick Roell testing equipment with strain rate of 1.6 mm/min at room temperature according to ASTM E8/E8M-21 (ASTM International Committee 2016).

Results and discussions

Weld's profile

The welds were made using different welding speeds, tool rotational speeds, and forces. The lower sheet was made of cast aluminium alloy, while the upper sheet was made of extruded Al 6063-T6. In all of the welds, the penetration was similar and equal to the height of the probe. Additionally, the stirring of materials was more pronounced on the advancing side (AS) due to the same linear speed of the pin and welding direction, which led to better mixing and more material flow. In FSW, there are several common defects, including lack of penetration, excessive flash, kissing bond, surface tunnelling, hook and root cavities, that can be prevented through process parameter optimization, as reported in the compressive review on FSW of aluminium alloys by Threadgilll et al. (2009). Simlialry Kah et al. (2015) investigated various types of welding defects particulary in FSW of aluminium alloys. However, in this particular study, the hook defect and root cavities were the most dominant defects. These defects are indicated in Fig. 3 with red and yellow arrows, respectively. The root cavities in the weld are generated due to lack of heat and material mixing at the probe tip inside the cast materials. The closer look of root cavity developed in sample S3 can be seen clearly in Fig. 3-g, whereas the closer look of typical microstructural features i.e., formation of hook and onion rings in sample S4 are visible in Fig 3-h.

It is clearly visible from Fig. 3 that in the first three welds, higher welding speeds caused big cavities in the weld's root, which were like a wormhole inside the SZ in the center and RS due to insufficient mixing of material and lack of frictional heat input. To achieve defect-free welds,

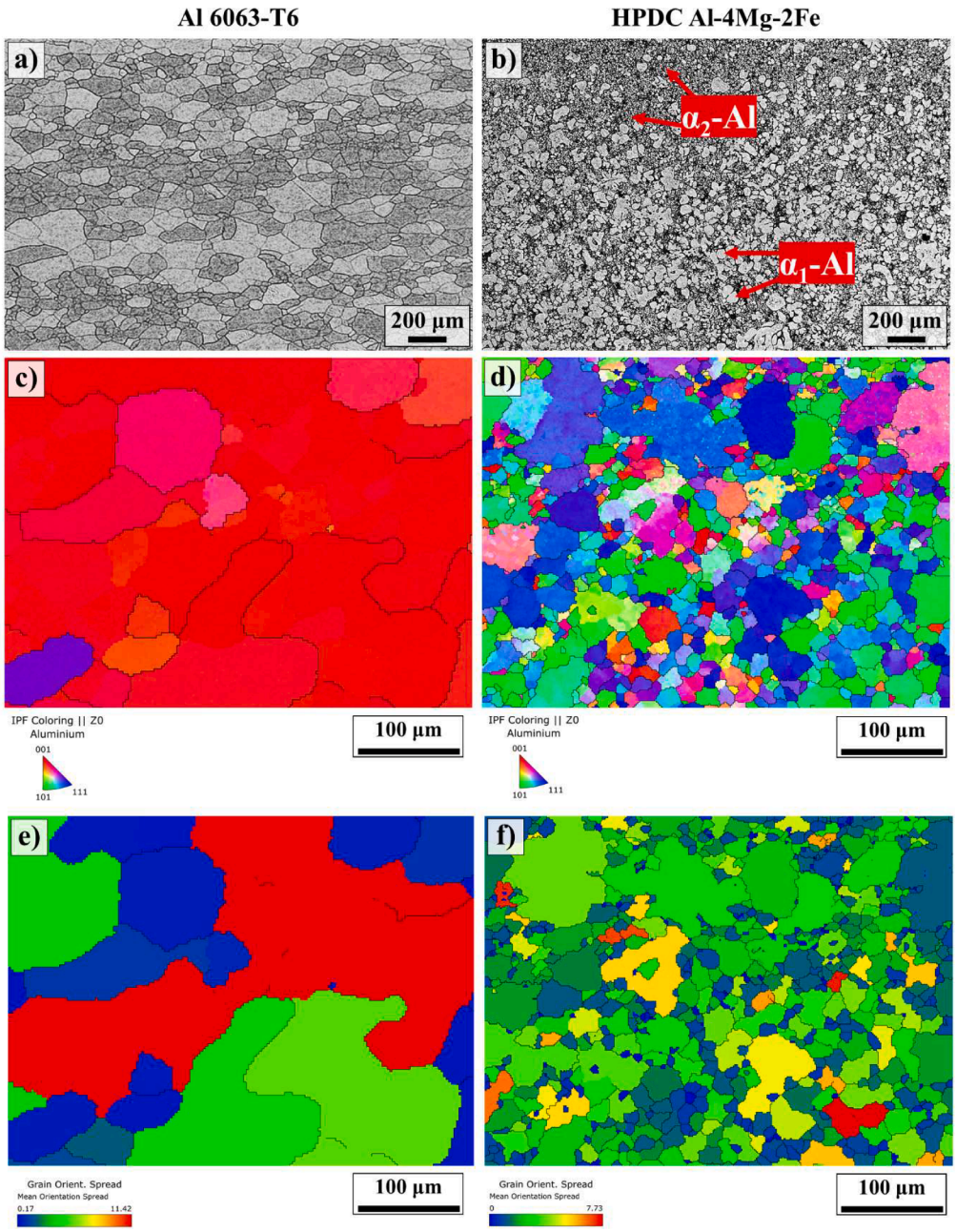

Fig. 5. Light optical microscopy and EBSD analysis of the base materials (extruded Al 6063-T6 and HPDC Al-4Mg-2Fe. (a, b) light optical micrographs. c, d) EBSD inverse pole figures (IPF) maps. (e, f) EBSD grain orientation spread (GOS) maps.

the welding speed was reduced, resulting in elimination of root cavity defects in the welds with lower welding speeds (S4, S5, and S6). In FSW, the heat input has the opposite relation to welding speed, and the reduction of welding speed increased heat input, resulting in better mixing and elimination of root cavity defects (Patel et al., 2022). In comparison of S1 and S3, welding defect should be mitigated by reducing the welding speed. But, in the given case, sample S3 was generated at lower welding force of 4500 N as compared to sample S1 (5000 N). Hence, welding force has demonstrated the great dominance on the defect formation in sample S3 as compared to sample S1. Additionally, the softening of the stirred material was boosted by the increment of heat input, allowing the stationary shoulder to better forge the material to suppress defect formation. The onion ring-like appearance of the SZ in the cross-sections of the welds with lower welding speed (S4, S5, and S6) demonstrates excellent material mixing of the upper and lower sheets, as well as strong bonding between them. The spacing of the onion rings is wider in the center compared to the edge due to the lower linear speed of the probe, and the process parameters have an influence on the hook height on both sides. Krishnan (2002) described the influence of the welding parameters on the formation of onion rings, claiming that the spacing of the onion rings is equal to the forward movement of the tool per rotation. This spacing, therefore, is wider in the center compared to the edge due to the lower linear speed of the probe. Increasing the probe rotational speeds from 1500 to 2000 rpm (welds S5 and S6) improved material mixing in the SZ and decreased the distance between two onion rings on the AS of the weld. Fereiduni et al. (2018) reported that tool rotational speed is also considered one of the most important parameters in FSW while mixing two completely different aluminium alloys.

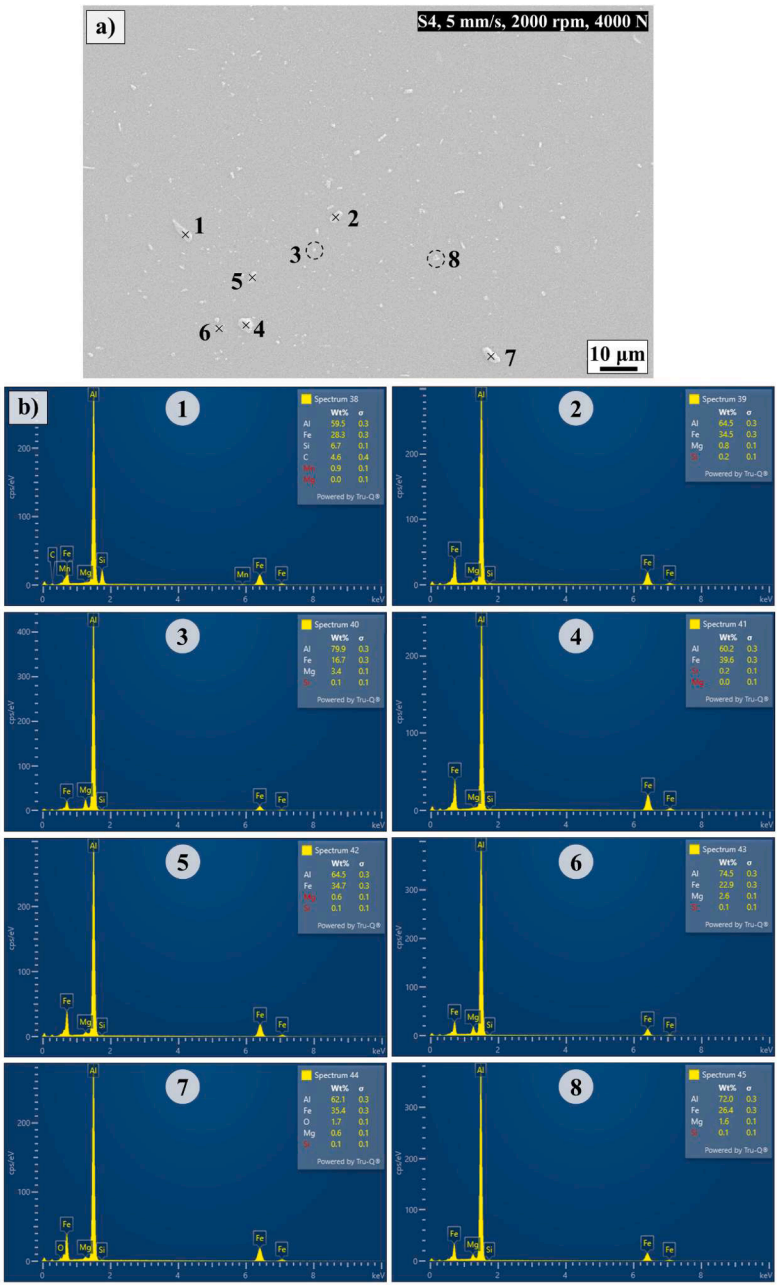

Fig. 6. (a) The SEM micrograph of the SZ. Inhomogeneous distribution of precipitates. (b) EDS analysis of the Stir zone.

Base materials microstructures

The microstructures analysis containing precipitates of base materials, extruded Al 6063-T6 and HPDC Al-4Mg-2Fe, are presented in Fig. 4. The microstructure of the HPDC Al-4Mg-2Fe alloy is affected by the high cooling rate during the casting process, which results in a non-equilibrium solidification and the formation of metastable phases (refer Fig. 4-b). The coarse and inhomogeneous precipitates in the HPDC Al-4Mg-2Fe alloy are mainly composed of Fe-rich intermetallic compounds such as β-Fe and Al_6(FeMn) phases, as well as Mg_2Si particles (Zajac et al., 1994). The SEM-EDS analysis in Fig. 4 confirms the presence of Fe and Si in the precipitate. The mechanical properties of HPDC Al-4Mg-2Fe alloy are generally lower than those of wrought aluminium alloys due to the presence of casting defects and the non-uniform distribution of the alloying elements in the microstructure (coarser precipitates). However, FSW has been shown to improve the mechanical properties of cast aluminium alloys by enhancing the microstructural homogeneity and reducing the size and distribution of casting defects. The EBSD analysis of the extruded Al 6063-T6 and HPDC revealed that the extruded alloy had a stronger ⟨100⟩ texture, whereas the cast alloy showed a more random crystallographic orientation (refer Fig. 5-c and -d). The ⟨100⟩ texture is formed during the extrusion process due to the shear deformation of grains in the direction of extrusion. The EBSD analysis also showed that the grain size of the extruded alloy was larger in the longitudinal direction of extrusion than in the transverse direction. The cast alloy, on the other hand, had a smaller grain size with more random grain orientations due to the rapid solidification during the casting process. The EBSD analysis also revealed the presence of sub-grains in the cast alloy, which is a common feature in rapidly solidified materials. The presence of sub-grains indicates that the grains in the cast alloy were not fully equilibrated and had undergone deformation during solidification. Overall, the microstructures and textures of the two base materials are significantly different due to their manufacturing processes and alloy compositions.

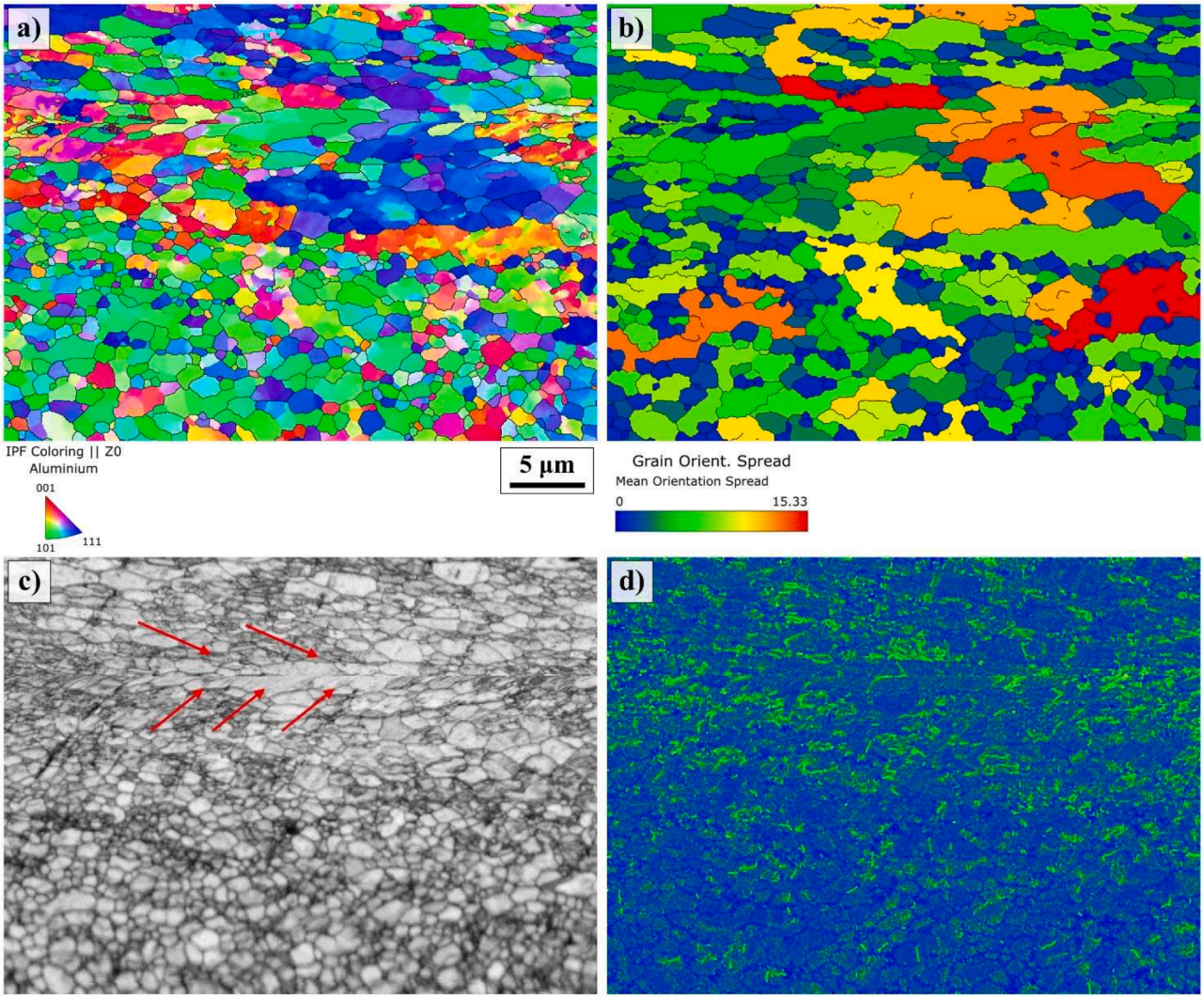

Fig. 7. EBSD analysis (a) inverse pole figures (IPF) map, (b) grain orientation spread (GOS) map, (c) band contrast (BC) map, and (d) kernel average misorientation (KAM) map from the center of the S4 weld SZ.

Weld metal microstructure

The S4 weld was selected for further microstructure characterization because it had a similar SZ to the other two defect-free welds (S5 and S6). The analysis was carried out in the center of the S4 weld SZ, as shown in Fig. 3. The SEM image in Fig. 6-a shows that the S4 weld SZ contains an aluminium matrix with fine precipitates dispersed throughout. The EDS analysis of these precipitates in Fig. 6-b indicates that the stirring action of the tool during welding caused the large Fe particles in the HPDC alloy to break, resulting in a significant decrease in precipitate size. The SZ microstructure can be classified into coarse and fine precipitates that were formed during the mixing of the extruded and cast alloys. As shown in Fig. 6, the coarse precipitates have a rod shape and are primarily composed of Al-Fe-Si with a significant amount of Fe particles. Some large precipitates in spherical shape were also formed, composed only of Al-Fe compositions. This suggests that the large plate-shaped Fe particles in the HPDC alloy were transformed into smaller, spherical and rod-shaped particles due to their breakage during welding. It is worth noting that the rotational speed of the welding tool (i.e., 2000 rpm) was high enough to break the Fe particles.

The EBSD analysis of the SZ in the S4 weld revealed several features, as presented in Fig. 7. The inverse pole figure (IPF) map in Fig. 7-a shows a severe reduction in grain size compared to the base materials, with two distinct grain types observed: larger grains orientated along the ⟨111⟩ direction and smaller grains along the ⟨101⟩ direction. The grain orientation spread (GOS) map in Fig. 7-b confirms that the smaller grains are the result of dynamic recrystallization, and it is a result of the heat and severe plastic deformation occurred in the SZ. The similar results on dynamic recrystallisation mechanism in FSW demonstrated in previous studies by Yu et al. (2021) and Etter et al. (2007). In this study, the high angle grain boundary (HAGB) in the SZ is approximately 74%, which is higher than that of the extruded alloy but lower than that of the cast alloy. The band contrast (BC) and kernel average misorientation (KAM) maps in Fig. 7-c and 7-d, respectively, reveal the effects of stirring and material flow on the grains and lattice structures. The BC map shows shearing, distortion, and strain in the grains and lattice structures due to the stirring action, while the KAM map indicates that the lattice strain is significantly reduced in the recrystallized area (i.e., the smaller grains) due to the rearrangement of dislocations. Additionally, comparing the IPF and BC maps shows that the small and large grains are representative of onion rings, as observed in Fig. 3-d. Overall, the EBSD analysis provides valuable insights into the microstructural changes that occur in the SZ during FSW.

Mechanical properties

To evaluate mechanical properties of the SSFSW, the hardness measurement and tensile tests were conducted on the welds. Hardness

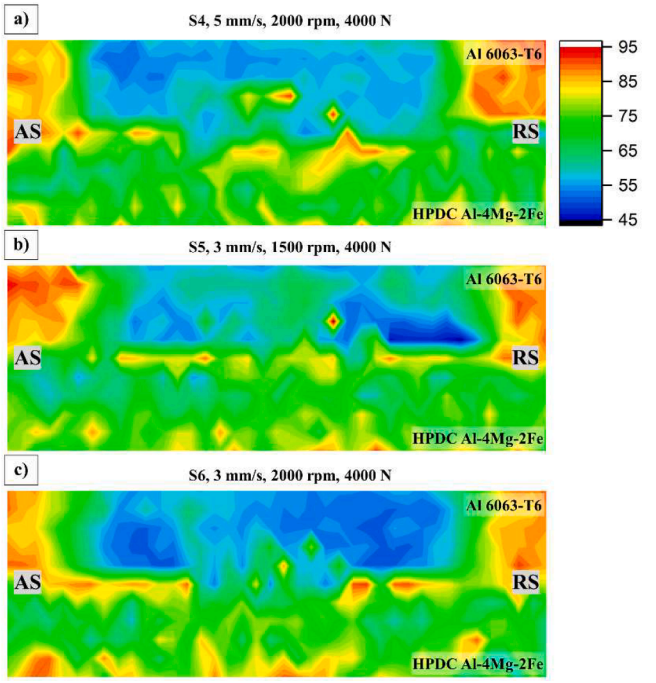

Fig. 8. Vickers hardness mapping of S4, S5, and S6 SSFSWs.

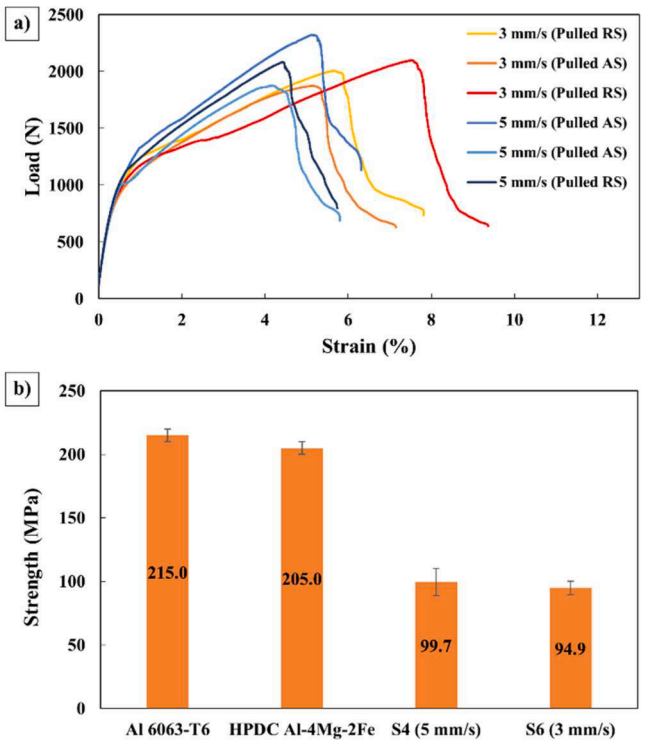

Fig. 9. Lap shear tensile test results of SSFSW joints: (a) tensile load curves and (b) strength bar diagram along with base materials.

mapping was conducted on defect-free welds (i.e., S4, S5, S6), whereas tensile testing was conducted for S4 and S6 for comparing the welding speed at same rotation speed (2000 rpm) and force (4000 N).

The hardness map representing the hardness value of distinct microstructural zones i.e., SZ, TMAZ, HAZ, and BM are illustrated in Fig. 8 (samples without root cavity defects, i.e., S4, S5, and S6). The hardness of the extruded Al 6063-T6 is higher than that of the HPDC due to the fine and dispersed precipitates present in the former. This difference in hardness is likely because the extruded Al 6063-T6 is processed using a different manufacturing technique that produces a finer grain structure and more uniformly distributed precipitates. It is also worth noticing that SZ region experienced reduction in the hardness for all three samples. This decrease in hardness is due to the mixing of two dissimilar alloys, which can lead to the formation of new phases, change in the distribution of precipitates, and dissolving/coarsening of fine precipitates during welding.

The extruded Al 6063-T6 has higher hardness than the HPDC Al-4Mg-2Fe due to the fine and dispersed precipitates in that. When two different base metals are mixed together in the SZ during SSFSW of dissimilar aluminium alloys, it can lead to a reduction in hardness values. This is mainly due to the mixing of two dissimilar alloys that can cause changes in microstructure and composition, which can affect the hardness. The hardness of aluminium alloys is affected by several factors such as the grain size, morphology, and distribution of precipitates, and weld heat input. Following three factors mainly affecting hardness in SSFSW of dissimilar aluminium alloys are discussed.

- The initial condition of the base materials is an essential factor in determining the hardness variation during FSW. In the case of dissimilar aluminium alloys, the hardness reduction is more pronounced in Al 6063-T6 compared to HPDC alloy. This is because the T6 heat treatment in Al 6063-T6 improves the strength of the alloy by forming fine precipitates, which are more susceptible to deformation during FSW. The formation of fine precipitates in Al 6063-T6 during the T6 heat treatment strengthens the alloy by hindering the movement of dislocations. Also, Liu et al. (2017) exhibited effect of T6 heat treatment on precipitation in AA6xxx alloy. However, during FSW, the high heat and pressure can cause these precipitates to deform and break down, resulting in a reduction in hardness. On the other hand, HPDC alloy, which is not subjected to heat treatment, contains larger and less-dispersed precipitates that are more resistant to deformation during FSW and, therefore, show less of a reduction in hardness. During SSFSW, the heat generated due to the friction between the tool and the base materials caused the fine precipitates in the alloy to dissolve, resulting in a hardness reduction in the SZ. Therefore, the choice of alloy and its initial condition, including the heat treatment and distribution of precipitates, should be carefully considered when performing SSFSW to minimize the detrimental effects of frictional heat on the hardness of the material.
- The second phenomenon is dynamic recrystallization (DRX), which occurs in FSW of aluminium alloys. DRX involves the nucleation and growth of new grains in the SZ due to the high temperature and deformation. This can have both positive and negative effects on the hardness and strength of the material. DRX can increase the hardness of the material by forming fine grains. These fine grains can hinder the movement of dislocations and improve the strength of the material. On the other hand, DRX can also decrease the concentration of dislocations, which can lead to a reduction in hardness. This is because dislocations are responsible for the plastic deformation of the material, and a reduction in their concentration can result in lower strain hardening. In the present study, the reduction in dislocation concentrations due to DRX overcame the grain refinement, resulting in a reduction in the hardness of the SZ. This emphasizes the complex interplay between grain refinement and dislocation concentration in determining the hardness and strength of dissimilar aluminium alloys joining.
- Ultimately, the effect of stirring and mixing can be observed in the SZ of SSFSW. The stirring and mixing action can cause the metal to undergo plastic deformation, which can lead to a reduction in its hardness. Moreover, the lateral area of the probe in the SSFSW tool experiences the highest linear speed of mixing during the process. This means that the metal in this area undergoes more deformation and has a greater reduction in hardness compared to the center of the

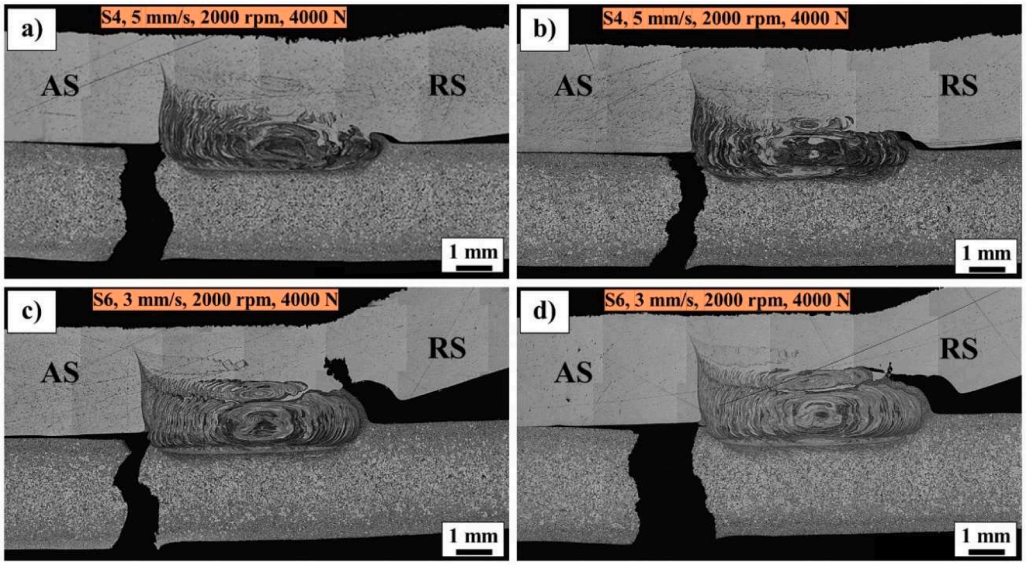

Fig. 10. Cross-sections of welds S4 and S6 after failure in tensile test. (a and c) pulled from RS. (b and d) pulled from AS.

SZ where the linear speed is lower. Therefore, the hardness reduction is more recognizable in the lateral area of the probe.

Furthermore, in the peripheral regions of the probe stirring, where the material is subjected to high temperatures due to friction, there is a slight softening of the TMAZ/HAZ. This could be related to the over-aging of the precipitates in these regions, which occurs due to the generated heat from friction during the FSW process. The HAZ is the area surrounding the FSW joint where the material has undergone heating but not plastic deformation. The TMAZ is the area immediately adjacent to the weld where the material has undergone both heating and plastic deformation. It is noteworthy that as the welding speed decreases from 5 to 3 mm/s (S4 and S6), there is a more pronounced reduction in the hardness of the SZ. This is likely a result of the increased heat input caused by the slower welding speed, leading to a more significant overaging effect in the material. In summary, the dominant factor influencing the hardness for the given joint configuration is heat imparted by the SSFSW tool based on the initial conditions of the BM.

The tensile shear test was conducted on two selected welds, S4 and S6, which were chosen based on the cross-sections of the welds in Fig. 3 and the hardness maps in Fig. 8. The load-strain curves of three samples from each of the two welding conditions are presented in Fig. 9-a. The results showed that there is no significant difference between the maximum tensile loads when the welds are pulled from the advancing side (AS) and the retreating side (RS) for the S4 weld. This indicates that the weld is homogeneous and has consistent mechanical properties throughout its structure. Interestingly, increasing the welding speed from 3 to 5 mm/s did not have any remarkable effect on the average tensile load of the welds. The similar mechanical properties of the S4 and S6 welds can be attributed to the similar mixing of materials in these two welds. This suggests that increasing the welding to 5 mm/s can increase productivity while having no considerable negative effects on the microstructure and mechanical properties of the welds. Overall, the results of the tensile shear test suggest that the SSFSW process can produce homogeneous welds with consistent mechanical properties, even when the welding speed is increased. This has important implications for the industrial application of SSFSW, as it suggests that higher welding speeds can be used without compromising the quality and reliability of the resulting welds.

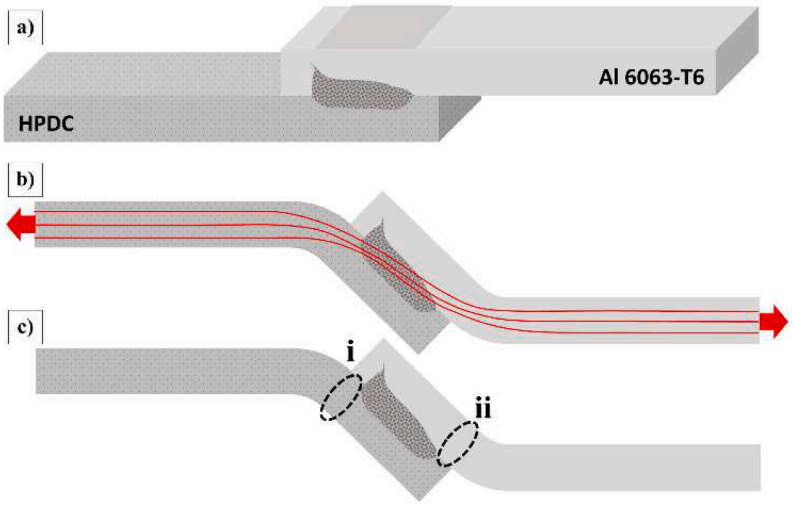

Fig. 11. Schematic illustration of (a) SSFSW HPDC Al-4Mg-2Fe to extrude Al 6063-T6, (b) Stress concentration in the weld and surrounding area, and (c) two probable area for fracture.

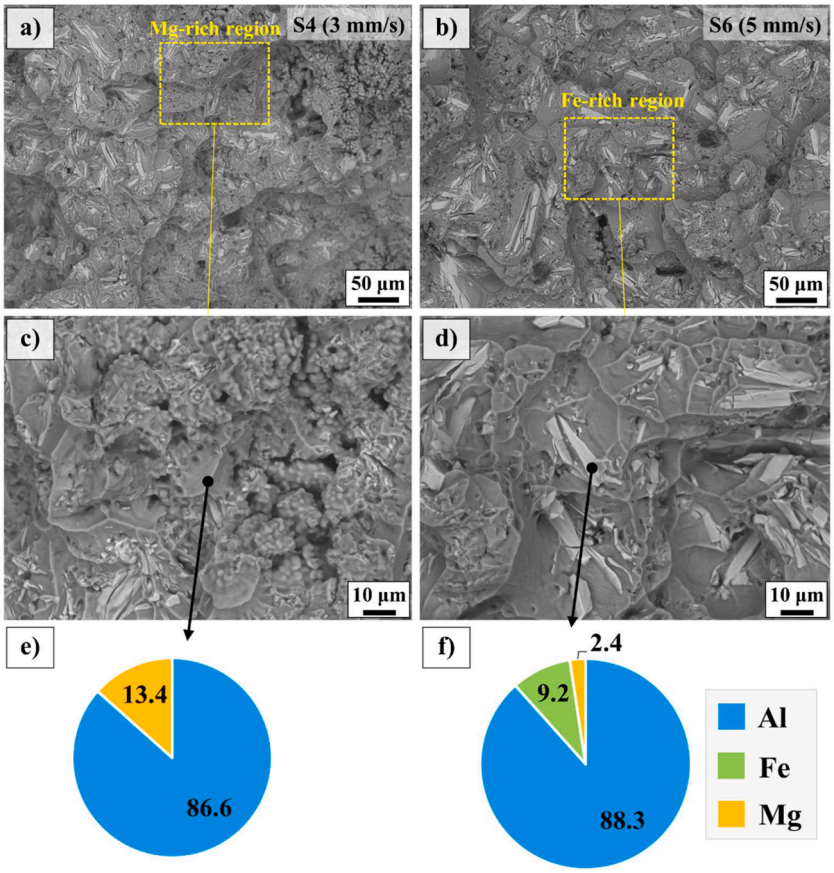

Fig. 12. The fracture surfaces of SSFSW welds: (a and c) S4: 3 mm/s, and (b and d) S6: 5 mm/s. (e and f) SEM-EDS analysis of specified locations.

Fracture location and fractography

In order to understand the fracture behavior of lap joints, the cross-sections of welds (sample S4 and S6) after tensile test are presented in Fig. 10. It is clearly evident from the cross-sections that both welds experienced crack initiation from the hook defect on the RS to the extruded aluminium alloy. However, the final failure of both welds occurred from the intersection of the hook defect and the lower sheet on the AS, into the lower sheet. This type of failure behavior is often observed in welded joints where there is a concentration of stress due to the presence of defects, such as the hook defect. These defects can act as stress concentrators, leading to crack initiation and propagation, ultimately resulting in failure. Similarly, Xue et al. (2011) reported fracture location in the HAZ of the aluminium (upper sheet) regardless of being in advancing or retreating sides in case of dissimilar combination of aluminium to copper lap joints. The main reason was lower hardness of the aluminium compared to copper. In fact, in dissimilar lap joint FSW of aluminium alloys, the fracture mostly happens in HAZ/TMAZ of the sheets with lower hardness and strength. These areas can be more susceptible to cracking and failure, especially if the material with lower hardness and strength is in the HAZ or TMAZ. As it is illustrated in Fig. 11-a and -b, the schematic of the weld before and during tensile test, the load transferring lines (red lines) developed stress concentration in the weld and adjacent areas. Two locations (i-ii, as shown in Fig. 11-c) are the most susceptible regions for fracture due to stress concentration and HAZ softening, and which is considered as common phenomenon in FSW of aluminium alloys similar to previous study reported by Lee et al. (2003).

As it can be seen in Fig. 8, the cast alloy has lower hardness and strength than the extruded alloy. In this study, the crack firstly initiated from location ‘ii’ at RS since the mixing of material was lower than the AS. In the end, it appears that there was an initial crack initiation at location "i" due to some stress or loading condition, which then propagated until failure occurred. Comparing the cross-sections of the weld revealed that increasing the welding speed resulted in a decrease in the opening of the RS during tensile testing. This could be due to the higher hardness of the S6 area compared to S4, which may have caused the material to resist deformation and crack propagation more effectively.

To evaluate fracture type, the fractured surface of the tensile specimens (Samples S4 and S6) was examined under the SEM (refer Fig. 12). Large number of dimples are observed in the fracture surfaces of both welds, which indicates an extensive plastic deformation occurred during the tensile test. As it can be seen similar fractured surface behavior for the both samples at lower magnification images in Fig. 12-a, b. But, higher magnification images (see Fig. 12-c, d) from the different regions are examined in order to know the presence of primary alloying elements at those two different location i.e., Mg- and Fe-rich fractured region as marked in Fig. 12-a, b. Furthermore, the presence of Mg and Fe elements are quantified through EDS analysis in Fig. 12(e. f). The EDS analysis confirmed the presence of Mg ang Fe elements in the respective regions. It is worth to observe that fracture surface at higher magnification (as shown in Fig. 12-d) that represents HPDC alloy. Moreover, it also exhibits typical size and shape of Fe particles alongside with different dimple sizes, representing respective α_1- and α_2-Al grains. Ductile fracture is a type of fracture that occurs in materials that can undergo plastic deformation before they break. Therefore, it can be concluded that fracture mode is ductile in the present study.

Conclusions

The present study aimed at dissimilar welding of extruded and cast aluminium alloys used for battery frame welding in BEV industry for

lightweight structure assembly. The study investigated the microstructures and mechanical properties of the lap welds made using stationary shoulder FSW, and following points are concluded:

1. Defect-free welds were produced by SSFSW with excellent materials mixing in the SZ at 3 and 5 mm/s welding speeds.
2. The grain size in the SZ drastically reduced as compared to both base materials, which demonstrated the remarkable DRX in this region.
3. The large iron particles of the HPDC alloy were broken by the rotating probe, and the weld comprised of fine dispersed precipitates.
4. The fracture occurred from the hook area in AS at the cast alloy due to its lower hardness and strength as compared to extruded alloy.
5. On increasing welding speed from 3 to 5 mm/s, the tensile strength and failure behviour remain almost similar. Hence, 5 mm/s welding speed is recommended to join dissimilar aluminium alloys using SSFSW for enhancing the productivity.

Declaration of Competing Interest

The authors declare that they have no known competing financial interests or personal relationships that could have appeared to influence the work reported in this paper.

Data availability

No data was used for the research described in the article.

Acknowledgments

The funding support from the VINNOVA project of EVASTIR (2019-03114) with industry partners Volvo Cars Corporations, Hydro Extruded Solutions, ESAB, and i-Weld project H2020-MSCA-RISE-2018 (Project number: 823786) are highly acknowledged.

References

Ahmed, M.M.Z., Wynne, B.P., Rainforth, W.M., Threadgill, P.L., 2011. Through-thickness crystallographic texture of stationary shoulder friction stir welded aluminium. Scr. Mater. 64, 45–48. https://doi.org/10.1016/j.scriptamat.2010.08.060.

Aldanondo, E., Arruti, E., Echeverria, A., 2017. Friction Stir Weld Lap Joint Properties in Aeronautic Aluminium Alloys. Springer International Publishing, Cham, pp. 109–117. https://doi.org/10.1007/978-3-319-52383-5_12.

ASTM International Committee. Standard test methods for tension testing of metallic materials. ASTM International; 2016.

Barbini, A., Carstensen, J., dos Santos, J.F., 2018. Influence of a non-rotating shoulder on heat generation, microstructure and mechanical properties of dissimilar AA2024/AA7050 FSW joints. J. Mater. Sci. Technol. 34, 119–127. https://doi.org/10.1016/j.jmst.2017.10.017.

Besharati-Givi, M.K., Asadi, P., 2014. Advances in Friction-Stir Welding and Processing. Elsevier Science & Technology, Cambridge. https://doi.org/10.1016/C2013-0-16268-X.

Çam, G., Mistikoglu, S., 2014. Recent developments in friction stir welding of Al-alloys. J. Mater. Eng. Perform. 23, 1936–1953. https://doi.org/10.1007/s11665-014-0968-x.

Dinaharan, I., Kalaiselvan, K., Vijay, S.J., Raja, P., 2012. Effect of material location and tool rotational speed on microstructure and tensile strength of dissimilar friction stir welded aluminum alloys. Arch. Civ. Mech. Eng. 12, 446–454. https://doi.org/10.1016/j.acme.2012.08.002.

Etter, A.L., Baudin, T., Fredj, N., Penelle, R., 2007. Recrystallization mechanisms in 5251 H14 and 5251 O aluminum friction stir welds. Mater. Sci. Eng. A 445–446, 94–99. https://doi.org/10.1016/j.msea.2006.09.036.

Fereiduni, E., Movahedi, M., Baghdadchi, A., 2018. Ultrahigh-strength friction stir spot welds of aluminium alloy obtained by Fe_3O_4 nanoparticles. Sci. Technol. Weld. Join. 23 https://doi.org/10.1080/13621718.2017.1356031.

Kah, P., Rajan, R., Martikainen, J., Suoranta, R., 2015. Investigation of weld defects in friction-stir welding and fusion welding of aluminium alloys. Int. J. Mech. Mater. Eng. 10 https://doi.org/10.1186/s40712-015-0053-8.

Krishnan, K.N., 2002. On the formation of onion rings in friction stir welds. Mater. Sci. Eng. A Struct. Mater. 327, 246–251. https://doi.org/10.1016/S0921-5093(01)01474-5.

Lee, W.B., Yeon, Y.M., Jung, S.B., 2003. Evaluation of the microstructure and mechanical properties of friction stir welded 6005 aluminum alloy. Mater. Sci. Technol. 19, 1513–1518. https://doi.org/10.1179/026708303225008068.

Liu, G., Wang, Q., Liu, T., Ye, B., Jiang, H., Ding, W., 2017. Effect of T6 heat treatment on microstructure and mechanical property of 6101/A356 bimetal fabricated by squeeze casting. Mater. Sci. Eng. A 696, 208–215. https://doi.org/10.1016/j.msea.2017.04.072.

Mishra, R.S., Ma, Z.Y., 2005. Friction stir welding and processing. Mater. Sci. Eng. R Rep. 50, 1–78. https://doi.org/10.1016/j.mser.2005.07.001.

Patel, V., De Backer, J., Hindsefelt, H., Igestrand, M., Azimi, S., Andersson, J., et al., 2022. High-speed friction stir welding in light weight battery trays for the EV industry. Sci. Technol. Weld. Join. 27, 250–255. https://doi.org/10.1080/13621718.2022.2045121.

Sejani, D., Li, W., Patel, V., 2021. Stationary shoulder friction stir welding–low heat input joining technique: a review in comparison with conventional FSW and bobbin tool FSW. Crit. Rev. Solid State Mater. Sci. 0, 1–50. https://doi.org/10.1080/10408436.2021.1935724.

Song, Y., Yang, X., Cui, L., Hou, X., Shen, Z., Xu, Y., 2014. Defect features and mechanical properties of friction stir lap welded dissimilar AA2024-AA7075 aluminum alloy sheets. Mater. Des. 55, 9–18. https://doi.org/10.1016/j.matdes.2013.09.062.

Thomas W.M., Nicholas E.D., Needham J.C., Murch M.G., Temple-Smith P., Dawes C.J. Friction stir butt welding, international patent application no. PCT/GB92 Pat Appl 1991.

Threadgilll, P.L., Leonard, A.J., Shercliff, H.R., Withers, P.J., 2009. Friction stir welding of aluminium alloys. Int. Mater. Rev. 54, 49–93. https://doi.org/10.1179/174328009X411136.

Xu, Z., Li, Z., Ji, S., Zhang, L, 2018. Refill friction stir spot welding of 5083-O aluminum alloy. J. Mater. Sci. Technol. 34, 878–885. https://doi.org/10.1016/j.jmst.2017.02.011.

Xue, P., Xiao, B.L., Wang, D., Ma, Z.Y., 2011. Achieving high property friction stir welded aluminium/copper lap joint at low heat input. Sci. Technol. Weld. Join. 16, 657–661. https://doi.org/10.1179/1362171811Y.0000000018.

Yu, P., Wu, C.S., Shi, L., 2021. Analysis and characterization of dynamic recrystallization and grain structure evolution in friction stir welding of aluminum plates. Acta Mater. 207 https://doi.org/10.1016/j.actamat.2021.116692.

Zajac, S., Hutchinson, B., Johansson, A., Gullman, L.O., 1994. Microstructure control and extrudability of Al–Mg–Si alloys microalloyed with manganese. Mater. Sci. Technol. 10, 323–333. https://doi.org/10.1179/mst.1994.10.4.323.